EFFECTS OF ELEVATED CO_2 ON GROWTH, CALCIFICATION AND SPECTRAL DEPENDENCE OF PHOTOINHIBITION IN THE COCCOLITHOPHORE *EMILIANIA HUXLEYI* (PRYMNESIOPHYCEAE)[1]

M. Rosario Lorenzo

Department of Ecology, Faculty of Sciences, University of Málaga, Bulevar Louis Pasteur s/n, Málaga 29071, Spain

Patrick J. Neale[2]

Smithsonian Environmental Research Center, 647 Contees Wharf Rd, Edgewater, MD 21037, USA

Cristina Sobrino

Department of Ecology and Animal Biology, Faculty of Sciences, University of Vigo, Campus Lagoas-Marcosende. 36310 Vigo, Spain

Pablo León

Marine Scotland Science, Marine Laboratory, 375 Victoria Road, Aberdeen, AB11 9DB, U.K

Víctor Vázquez

Department of Ecology, Faculty of Sciences, University of Málaga, Bulevar Louis Pasteur s/n, Málaga 29071, Spain

Eileen Bresnan

Marine Scotland Science, Marine Laboratory, 375 Victoria Road, Aberdeen, AB11 9DB, U.K

and María Segovia

Department of Ecology, Faculty of Sciences, University of Málaga, Bulevar Louis Pasteur s/n, Málaga 29071, Spain

[1] Submitted XXXXXXXX Accepted XXXXXX

27 [2]Corresponding author, nealep@si.edu, 1-443-482-2285, Fax 1-443-482-2380

28 Running Title: Elevated CO_2 Effects on a Coccolithophore

Abstract

We studied the effects of elevated CO_2 concentrations on cell growth, calcification and spectral variation in the sensitivity of photosynthesis to inhibition by solar radiation in the globally important coccolithophore *Emiliania huxleyi*. Growth rates and chlorophyll *a* content per cell showed no significant differences between elevated (800 ppmv) and ambient (400 ppmv) CO_2 conditions. However, the production of organic carbon and the cell quotas for both, carbon and nitrogen, increased under elevated CO_2 conditions whilst particulate inorganic carbon production rates decreased under the same conditions. Biometric analyses of cells showed that coccoliths only presented significant differences due to treatments in the central area width. Most importantly, the size of the coccosphere decreased under elevated CO_2 conditions. The susceptibility of photosynthesis to inhibition by ultraviolet radiation (UVR) was estimated using biological weighting functions (BWFs) and a model that predicts photosynthesis under photosynthetically active radiation (PAR) and UVR exposures. BWF results demonstrate that the sensitivity of photosynthesis to UVR was not significantly different between *E. huxleyi* cells grown under elevated and present CO_2 concentrations. We propose that the acclimation to elevated CO_2 conditions involves a physiological mechanism of regulation and allocation of energy and metabolites in the cell, which is also responsible for altering the sensitivity to UVR. In coccolithophores this mechanism might be affected by the decrease in the calcification rates.

Keywords: Phytoplankton, Ocean Acidification, Calcification, Photoinhibition, *Emiliania huxleyi*

Abbreviations: AIC, Akaike Information Criterion; BWF, Biological Weighting Function; CAL, Central Area Length; CAW, Central Area Width; DIC, Dissolved Inorganic Carbon; DSA, Distal Shield Area; DSL, Distal Shield Length; DSW, Distal Shield Width; PIC, Particulate Inorganic Carbon; POC, Particulate Organic Carbon;

PON, Particulate Organic Nitrogen; RCP, Representative Concentration Pathway; RMSE, Root Mean Square Error; TPC, Total Particulate Carbon; UVA, UV radiation 320-400 nm; UVB, UV radiation 280-320 nm; UVC, UV radiation <280 nm; UVR, UV radiation 280-400 nm

Introduction

The atmospheric concentration of carbon dioxide (CO_2) has increased by 40% since pre-industrial times due to anthropogenic activities. The 5th IPCC report (IPCC 2014) predicts an increase in atmospheric CO_2 concentration above 1000 ppmv by the end of this century for the worst-case scenario (Representative Concentration Pathway (RCP) 8.5). Unfortunately, the values predicted by the RCP 8.5 match the measured concentrations in the atmosphere to date. The ocean is absorbing most of anthropogenic emissions of CO_2, which not only affects the quantity and speciation of the dissolved inorganic carbon (DIC) in the ocean, but also decreases the pH of the seawater (Doney et al. 2009). These changes in pH affect biogeochemical processes in marine ecosystems (Hoffmann et al. 2012) and have direct impacts on the physiological responses of primary producers such as phytoplankton (Kroeker et al. 2013, Mackey et al. 2015, Riebesell & Tortell 2011).

Phytoplankton play a key role in determining the effects of environmental change on the ocean surface since they are responsible for around 50% of the net amount of carbon assimilated annually by photoautotrophs (Field et al. 1998). Apart from acidification, global warming enhances stratification, which reduces nutrient availability in the surface mixed layer (Boyd & Doney 2002, Polovina et al. 2008). The surface mixed layer depth, which determines average exposure of phytoplankton to both ultraviolet (UV) and photosynthetically available radiation (PAR), reflects a balance between stratification and various physical forces propelling vertical mixing, all of which are affected by global change (Neale & Smyth 2018). Future shifts in this balance are expected to be regionally dependent (Boyd & Doney 2002, Somavilla et al. 2017). Phytoplankton will then be exposed to increasing CO_2 concentrations, low nutrient concentrations and regionally variable changes in average surface layer irradiance.

Among phytoplankton functional groups, coccolithophores have been widely studied due to their capability for producing calcium carbonate coccoliths (Paasche 2002). They are responsible for contributing to the sequestering of atmospheric CO_2 into chalk, changing both the atmosphere and geology of the Earth, over geological time-scales (Brown et al. 2004, Young et al. 2005). *Emiliania huxleyi* is a global model organism, keystone of the coccolithophores. It is widely distributed and forms extensive blooms in nutrient-depleted waters after the formation of the summer thermocline (Holligan et al. 1993). This model species is the most numerically important coccolithophore and a major primary producer in the world's oceans (Paasche 2001). *Emiliania huxleyi* is of paramount significance in the global carbon cycle by contributing ca. 1–10% to total organic carbon fixation and to approximately half of the pelagic deep ocean $CaCO_3$ sediments (Paasche 2001). Thus, it participates in the regulation of the exchange of CO_2 across the ocean−atmosphere interface through the rain ratio (the ratio of particulate inorganic to organic carbon in exported biogenic matter (calcite: POC or PIC: POC) (Rost & Riebesell 2004). A recent meta-analysis study demonstrates that the effect of ocean acidification on coccolithophores is species specific (Meyer & Riebesell 2015). In particular, elevated CO_2 has a negative effect on *E. huxleyi* calcification process, thus affecting the cellular PIC/POC ratio (Kroeker et al. 2013, Meyer & Riebesell 2015). The study of fundamental species such as *E. huxleyi* subjected to global change drivers, will help us to unravel the physiological processes that will govern the C-cycle and the biological pump in future scenarios of global change.

Global change also affects exposure of phytoplankton in surface waters to solar ultraviolet B (UVB, 280–320 nm), ultraviolet A (UVA, 320–400 nm) and photosynthetically available radiation (PAR, 400-700 nm) through changes in the stratospheric ozone concentration, cloud cover and levels of dissolved organic matter

(Bais et al. 2018). Stratospheric ozone loss due to anthropogenic emission of chlorofluorocarbons, now limited by the Montreal Protocol, was an important cause for increased UVB in the latter decades of the 20th century (around 6% in the Northern Hemisphere). This level of depletion is persisting into the 21st century due to the long time required for ozone recovery (Bais et al. 2015, Shanklin 2010). The future course of ozone depletion depends on the interactive effects with other global change drivers that are also affecting stratospheric dynamics and temperature (Weatherhead & Andersen 2006).

Both UVB and UVA (together – UVR) cause deleterious effects on the physiological performance and growth of marine phytoplankton and other organisms (Häder 2011). The estimation of the sensitivity to UVR exposure in relation to wavelength can be quantified by biological weighting functions (BWFs) (reviewed by Neale (2000)). They allow comparison between responses to different wavelengths of UVR as well as PAR and can predict the effects of irradiance variations due to global change using the appropriate exposure response model.

Changes in several variables may not result in simple additive responses relative to that occurring by a given variable alone (Boyd & Hutchins 2012). Combined change can produce either synergistic, antagonistic or neutral effects (Folt et al. 1999). Accordingly, it has been observed that the effects of UVR on marine primary producers are modulated by other environmental factors such as light availability, nutrient limitation and levels of dissolved CO_2 (Beardall et al. 2009, Beardall et al. 2014). Specifically, increased CO_2 concentrations affect the sensitivity of phytoplankton photosynthesis to inhibition by solar, and in particular UV irradiance (Gao et al. 2009, Gao et al. 2012, Sobrino et al. 2005, Sobrino et al. 2009, Sobrino et al. 2008). Previous

studies have not shown a unique pattern of the interactive effects of UVR and increased CO_2, instead that such effects depend on the species. This suggests that the interactions between elevated CO_2 and UVR may produce changes in the taxonomic composition of phytoplankton assemblages (Beardall et al. 2009). The essential question is to understand the response of phytoplankton physiology to the environmental conditions in order to assess whether the effects of the variables are synergistic, antagonistic or neutral.

The aim of this work was to analyze the effects of elevated CO_2 conditions on *E. huxleyi* growth, photosynthesis and calcification under non-photoinhibitory and photoinhibitory exposures in order to understand its physiological response to future scenarios of ocean acidification. The strain selected for this study is a heavily calcified Type A strain isolated from the Norwegian Sea. Specifically, we analysed the physiological behaviour of this species through the assessment of exposure response curves and spectral dependence weighting functions (BWFs) for UV and PAR inhibition of photosynthesis.

Material and methods

Culture growth conditions

Cultures of the coccolithophore *Emiliania huxleyi* (Lohmann) Hay & Mohler, Haptophyta, were provided by the Roscoff Culture Collection (RCC #1226) and grown in semi-continuous culture at 16°C with constant aeration in two different treatments: (1) ambient CO_2 (400 ppm CO_2) and (2) elevated CO_2 (800 ppm CO_2). Cultures were maintained in exponential growth conditions for at least 14 days before experiments were conducted. The gas mixture for the elevated CO_2 was provided by Air Products,

160 Inc (Allentown, PA, USA). Aeration with 800 ppm CO_2 changed the pH of the media
161 from 8.14 to 7.84. The partial pressure of CO_2 (p CO_2) in the two conditions was
162 verified by measuring the pH, temperature and salinity in the seawater and determining
163 dissolved inorganic carbon (DIC) in a Shimadzu TOC-V analyser. These results were
164 used with the CO_2SYS program to calculate the equilibrium concentrations of dissolved
165 CO_2, bicarbonate and carbonate (Zeebe & Wolf-Gladrow 2001). Growth irradiance was
166 provided by cool white fluorescent lamps on a 14 h light:10 h dark photoperiod at an
167 irradiance of 170-180 μmol photons m^{-2} s^{-1}. Growth PAR was measured with a 4-π
168 probe (QSL-2100, Biospherical Instruments) immersed in distilled water inside the
169 culture flasks. The growth medium consisted of filtered seawater from the Sargasso Sea
170 enriched with f/2 nutrients with Fe concentration reduced by half (Guillard & Ryther
171 1962). The experiments were carried out in the middle of exponential growth phase and
172 repeated at least three times with independently grown cultures for each treatment. Cell
173 numbers were counted every day with a Neubauer hematocytometer. The growth rate
174 (μ, d^{-1}) was calculated as ln (N_2/N_1)/t, where N_1 and N_2 are the cell concentrations, and t
175 is the time between samples (d).

176 *Maximum photosynthetic efficiency of PSII*

177 A pulse amplitude–modulated fluorometer Diving PAM/B (Walz) with a blue light-
178 emitting-diode (LED; 470 nm) excitation was used to assess the maximum
179 photosynthetic efficiency of the cultures at different times during the experiment. A
180 custom fabricated acrylic "light-pipe" enabled fluorescence measurements directly on
181 the culture flask with sufficient signal/noise ratio. The data are expressed as the
182 photosystem II (PSII) quantum yield, $F_v:F_m = (F_m - F_0):F_m$, which has been correlated
183 with the maximum quantum yield of photosynthesis (Genty et al. 1989). F_0 is the
184 steady-state yield of *in vivo* chlorophyll a fluorescence in dark-adapted phytoplankton,

185 and F_m is the maximum yield of fluorescence obtained from an illuminated sample after
186 a saturating light pulse (400-ms pulse duration) has been applied. The light for the
187 saturating pulse, emitted by a halogen lamp, passed through a dichroic short-pass filter
188 with 580 nm cutoff (Balzers DT Cyan).
189 *Chlorophyll concentration and cellular absorbance*
190 Chlorophyll concentration was measured on aliquots concentrated on glass-fiber filters
191 (GF/F, Whatman Inc.) and extracted with 90% acetone overnight at -20ºC. After
192 extraction, fluorescence was measured before and after acidification on a Turner 10-AU
193 fluorometer. The fluorometer was calibrated with chlorophyll *a* (Sigma Chemicals).
194 Pigment absorbance ($a^*(\lambda)$, m^2 mg chl^{-1}) was measured using the quantitative filter
195 technique (QFT) as described in Cleveland and Weidemann (1993) with modifications
196 as described by Tzortziou (2004). Cells concentrated on the filters were scanned from
197 280 to 750 nm in a Cary 4 dual-beam spectrophotometer, using a blank filter wetted
198 with filtrate as a reference. The filter was extracted with 100% methanol, washed with
199 filtrate, and rescanned using a similar procedure as for the non-extracted filter.
200 *Photosynthesis measurements*
201 The photosynthetic response to solar radiation was performed using a polychromatic
202 incubator illuminated with a 2.5 kW xenon lamp ("photoinhibitron"), based on the
203 design of Cullen et al. (1992) with modified block construction similar to that described
204 by Smyth et al. (2012). Details of the photoinhibitron are given in Neale et al. (2014).
205 The incubator provides treatment irradiance with PAR, UVA and UVB in similar
206 proportions as solar irradiance, allowing the assessment of realistic responses. Long-
207 pass filters combinations were used to define a total of 12 spectral treatments per
208 incubation, which were combined with neutral density screens to produce ten
209 irradiances per filter combination for a total of 120 treatments of varying spectral
210 composition and irradiance. The filter combinations are listed in the supplemental

information Table S1. Spectral irradiance (mW m^{-2} nm^{-1}) for each position in the photoinhibitron was measured with a custom-built fiber-optic spectroradiometer as described by Neale and Fritz (2001).

Photosynthesis was measured as total ^{14}C assimilation of added inorganic $H^{14}CO_3^-$ (~25 kBq mL^{-1}) into organic compounds (acid-stable) in 1 mL aliquots during 1 h incubation. Temperature was controlled using a circulating water bath. Data were fit to BWF/P-E functions:

$$P^B = P_s^B \left(1 - e^{-\frac{E_{PAR}}{E_s}}\right) ERC(E_{inh}^*) \quad \text{Equation 1}$$

$$E_{inh}^* = \sum_{\lambda=265}^{400} \varepsilon(\lambda) E(\lambda) \Delta\lambda + \varepsilon_{PAR} E_{PAR}$$

where P^B is the photosynthetic rate per unit chlorophyll (µg C µg chl^{-1} h^{-1}), P_s^B is the light-saturated rate of photosynthesis, ERC is, in a general sense, the exposure response curve for inhibition of photosynthesis which is formulated accordingly depending on the model chosen for fitting the observed responses. E_{inh}^* is a dimensionless index for biologically effective or weighted irradiance, $\varepsilon(\lambda)$ is the biological weight of inhibitory effect of UV (m^2 mW^{-1}) at wavelength λ (nm) and ε_{PAR} is the biological weight of inhibitory effect of PAR (m^2 mW^{-1}). $E(\lambda)$ is spectral irradiance (mW m^{-2} nm^{-1}) at λ (265-400 nm) and E_{PAR} is PAR irradiance (W m^{-2}). Since responses to UVC (λ < 280 nm) are not relevant to present day conditions, we only report results for λ > 280 nm (cf. Neale et al., 2014). BWFs were estimated from the measured rates of photosynthesis using non-linear regression and principal component analysis (PCA). Details of the principal-component-based estimation procedure and error assessment are given in Cullen and Neale (Cullen & Neale 1997). Standard errors for the parameter means were calculated as the root mean square (rms, quadrature) of the estimation

standard errors (propagated from regression standard errors) and the standard error due to between-replicate variability. The BWF fits were performed using three different response models (ERCs) to determine the proper exposure – response model at high exposure. The *E* model (Eq. 2) was the model first developed to describe responses to UV as measured in the photoinhibitron (Cullen et al. 1992) and assumes that the specific rate of processes that restore photosynthesis ("repair") is proportional to the cumulative inactivation of photosynthetic components ("damage"):

$$\frac{P^B}{P^B_{pot}} = \frac{1}{1+ E^*_{inh}} \qquad \text{Equation 2}$$

where P^B_{pot} is the potential rate of photosynthesis in the absence of inhibition (i.e. the product of the first two terms of the Eq. 1 for P^B). The *T* model determines the presence of a threshold ($E^*_{inh} = 1$) above which, by definition, photosynthesis is inhibited (Eq. 3). It was developed to represent the ERC in which repair is considered to operate at a constant rate (Sobrino et al. 2005):

$$\frac{P^B}{P^B_{pot}} = \begin{cases} 1 & E^*_{inh} \leq 1 \\ \frac{1}{E^*_{inh}} & E^*_{inh} > 1 \end{cases} \qquad \text{Equation 3}$$

And finally, the E_{max} model uses a combination of the *E* model at low exposures and *T* model at high exposures ((Neale et al. 2014), Eq. 4). The new E^*_{max} parameter defines the transition between the exposure range over which repair rate increases with damage and higher exposures for which repair rate is constant (i.e., operating at some maximum rate).

$$\frac{P^B}{P^B_{pot}} = \begin{cases} \frac{1}{1 + E^*_{inh}} & E^*_{inh} \leq E^*_{max} \\ \frac{1}{cE^*_{inh}} & E^*_{inh} > E^*_{max} \end{cases}$$

$$c = \frac{1+ E^*_{max}}{E^*_{max}} \qquad \text{Equation 4}$$

A scaling coefficient, *c*, makes the function continuous at the E^*_{max} transition. A schematic representation of the relation between repair and damage of each of the models is shown the Supplemental Information (see Figure S1). The E_{max} model has an additional parameter compared to the *E* and *T* model. Whether sufficient increase in explained variance is gained to justify the incorporation of an additional parameter was assessed by evaluation of the Akaike information criterion (AIC) for each of the fits using the Matlab NonLinearModel function (Statistics toolbox).

Elemental composition: Particulate organic carbon and nitrogen quotas

For elemental composition analyses, cells were filtered onto pre-combusted GF/F filters (Whatman). To determine cellular particulate organic carbon (POC) quotas, respective filters were fumed with concentrated HCl overnight to remove calcite. Cellular particulate inorganic carbon (PIC) quotas were assessed as the difference in carbon content between HCl-treated (POC) and untreated filters (total particulate C, TPC). Particulate organic nitrogen (PON) was also measured in all filters.

Primary production and calcification rates

The relative rates of POC and PIC production, primary production and calcification respectively, were additionally determined by following the microdiffusion technique (MDT), (Paasche & Brubak 1994, Poulton et al. 2010), which allows the comparison of the responses from the same experimental sample. Samples (20 mL) of each independent culture (n=3) were inoculated with $H^{14}CO_3^-$ (approximately 37 kBq mL^{-1} final concentration) and incubated in triplicate at growth irradiance and temperature conditions. Incubations were ended after 2 hours by filtration under low-vacuum pressure through polycarbonate filters (25-mm diameter, 0.2-µm pore size), which were then rinsed with 0.2-µm filtered seawater to remove the non-incorporated ^{14}C-labelled DIC. Filters were then placed in the bottom of 20- mL scintillation vials that were

hermetically closed keeping inside a glass-fiber Whatman filters (GF/F) soaked with 0.2 mL ß -phenylethylamine (Sigma) located in the screw cap. Phosphoric acid (1 mL, 1%) was added into the bottom of the vial to convert ^{14}C-labeled calcite into $^{14}CO_2$, which was then sequestered by the ß-phenylethylamine–soaked GFF filter. When all the PIC was converted into $^{14}CO_2$ and trapped in the soaked filter (i.e. after 24 h), the CO_2 trap filters were removed and placed in fresh scintillation vials. Both, primary production and calcification rates were determined after the addition of scintillation cocktail (Insta-gel, Perkin Elmer), by using a scintillation counter LS-6599 (Beckman), and referred to the total inorganic carbon content of the incubation media used. Activity was checked by removal of 20 µL from each replicate after the spike addition, mixing with 0.2 mL of ß-phenylethylamine and liquid scintillation cocktail, and counting on the scintillation counter. $^{14}CO_2$ capture efficiency was ~ 93% and it was assessed by adding a spike of a known ^{14}C activity to seawater samples and determining the activity collected on the Whatman GFF filter relative to the spike activity. The average relative standard deviation (SD divided by mean x 100) of triplicate measurements was 7.6% for POC production and 7.9 % for PIC production.

Biometric analysis

For scanning electron microscopy (SEM) analyses, 1 mL of sample was concentrated onto a polycarbonate filter (0.8 µm pore-size). Filters were mounted on aluminium SEM stubs and sputter-coated with gold/palladium. (Quorum Q150T ES, Quorum Technologies Ltd., East Grinstead, UK). Filters were examined using a Carl Zeiss Evo ® MA10 SEM at the Institute of Medical Sciences (University of Aberdeen) Coccospheres and coccoliths morphometrics were measured from SEM digital images using Fiji-ImageJ 1.47v (National Institutes of Health, USA) analysis program. Measurements of *E. huxleyi* coccoliths focused on the distal shield, including the distal shield length (DSL), distal shield width (DSW), central area length (CAL), central area

width (CAW) and the number of slits (Supplementary Material Figure S2). The surface area of the distal shield (DSA) was estimated from DSL and DSW according to Bach et al. (2012)):

$$DSA = \pi \times \frac{DSL \times DSW}{4}$$

This equation assumes that the shield in an ellipse with semi-axes of DSL/2 and DSW/2. The outer shield length (OSL) was calculated assuming an elliptical shape of the coccolith as:

$$OSL = \frac{DSL - CAL + DSW - CAW}{4}$$

In addition, coccosphere diameter was also measured. Mean values of measured parameters were constant when counting more than 20 coccospheres / coccoliths per sample, so this number can be considered as statistically significant (Triantaphyllou et al. 2010).

Statistical analyses

Significant differences between treatments were analyzed using a t-test considering $p<0.05$ as significant. BWFs were estimated for each experiment, and the mean BWF was calculated for each treatment (n = 3–4), with standard errors for the mean derived from individual error estimates by propagation of errors.

Results

Particulate organic carbon and nitrogen quotas increased under elevated CO_2

The cellular characteristics of *E. huxleyi* cultures maintained in ambient and elevated CO_2 concentrations are shown in Table 1. Although elevated CO_2 did not affect growth rates or cellular chl content, POC and PON quotas were statistically different from ambient cultures. When grown with elevated CO_2, *E. huxleyi* increased its bulk POC

content relative to chl *a* by 15% ($p<0.001$) (Table 1). For the same samples, PIC content did not show significant differences between treatments. The PIC:POC ratio was lower under elevated CO_2 but the difference was not significant. The PON content was also significantly higher in elevated CO_2 conditions, but the increase was less than the increase in POC, so the POC:PON ratio was significantly higher (9%) in the elevated CO_2 conditions ($p = 0.035$). The average of F_v/F_m was the same (0.60 ± 0.01) for both conditions, showing that elevated CO_2 concentrations did not diminish the physiological performance of *E. huxleyi*. Cellular spectral absorbance normalized to chl *a* (*a**, Figure 1), also had a similar shape between treatments and was low in the UV, suggesting the absence of UV-absorbing compounds. Average *a** was lower for cultures in the elevated treatment but the difference with the ambient treatment was not significant (*t* test at 440 nm).

Organic and inorganic carbon production rates showed opposed trends with elevated CO_2

The assessment of carbon production rates in *E. huxleyi* using the microdiffusion technique showed that PIC production rates (mean ± SD) significantly decreased (13%, Figure 2A) from 2.12 ± 0.18 µg C µg chl a^{-1} h^{-1} in ambient CO_2 cultures to 1.85 ± 0.13 µg C µg chl a^{-1} h^{-1} in elevated CO_2 cultures ($p = 0.002$). On the contrary, POC fixation rates in the same samples increased by 15% ($p<0.001$), changing from 2.17 ± 0.16 to 2.54 ± 0.19 µg C µg chl a^{-1} h^{-1} in the elevated CO_2 cultures (Figure 2B). The PIC:POC production ratio showed a significant 25% decrease in elevated CO_2 cultures ($p<0.001$, Figure 2C) and changed from a 49%:51% contribution in the cultures grown under ambient conditions to a 42%:58% in the cultures acclimated to elevated CO_2.

These rates are somewhat different from the expected average production rates given the measured quotas (Table 1), which can be predicted as the product of growth rate and

359 quota averaged over the 14 hour light period. This assumes balanced growth which
360 should be approximated for exponential growing semi-continuous cultures (Balch et al.
361 1996). The predicted PIC rates (µg C µg chl a^{-1} h^{-1}) are about half of the MDT rates,
362 0.91±0.11 (ambient) and 0.93±0.09 (elevated). On the other hand the predicted POC
363 rates are slightly greater than the MDT rates, 2.47±0.25 and 2.82±0.15 µg C µg chl a^{-1}
364 h^{-1} for ambient and elevated respectively. The possible causes for this discrepancy are
365 considered in the discussion section.
366
367 *Coccoliths were affected by elevated CO_2*
368 Selected morphometric parameters measured in the coccoliths and the coccospheres are
369 presented in Table 2. Representative micrographs are shown in SI figure S3. The
370 coccoliths only showed significant differences between treatments in the central area
371 width (CAW, SI Figure S2 illustrates where dimensions were taken on the coccolith).
372 For cells acclimated to elevated CO_2, the CAW of the coccoliths showed a small, but
373 significant, increase, in addition to a slight increase in the central area length (CAL,
374 Table 2). Despite these differences, the coccoliths of cells grown in the two treatments
375 appear very similar in SEM micrographs (Figure S3 C, D). The increase in CAL was
376 not significant, neither were differences in the distal shield length (DSL) or distal shield
377 width (DSW). The size of coccolith's central area is inversely related to the area of
378 calcification (i.e. the region between the slits and the central area; Triantaphyllou et al.
379 2010). Thus, an increase in the central area reflects a decrease in the region of
380 calcification. Further analysis of the whole coccosphere showed that the coccosphere
381 diameter was also significantly different between treatments ($p<0.05$), with the size of
382 the coccosphere smaller under elevated CO_2 conditions.
383
384 *Elevated CO_2 did not increase UVR sensitivity*

385 The average rates of photosynthesis of *E. huxleyi vs*. irradiance measured using the
386 photoinhibitron were similar ($p>0.05$) between ambient and elevated CO_2 for all
387 spectral treatments (Fig. 3). These results allowed the estimation of biological weighting
388 functions (BWFs) for the inhibition of photosynthesis in cells grown under ambient and
389 elevated CO_2 conditions. We tested the fit of three possible exposure response curve
390 (ERC) models (*E*, *T* and E_{max}) to the response of *E. huxleyi* to UV and PAR exposure.
391 Figure 4 shows a representative set of observed photosynthetic rates and predicted
392 values using the estimated rates for the best fit obtained for each of the three BWF/P-E
393 models, where photosynthesis normalized to chl *a* (P^B) is plotted versus weighted
394 irradiance (E^*_{inh}, dimensionless). All three models provided good estimates of the
395 overall response with $R^2 > 0.89$ (n = 120), but there were systematic biases specific to
396 each model. The *E* model tended to underestimate observed rates at moderate exposures
397 ($1< E^*_{inh} <2$), while overestimating rates at high exposures ($E^*_{inh} >4$, Figure 4 a) and
398 showed the lowest value of R^2. In comparison, *T* and E_{max} models showed better
399 agreement with observed rates for exposures above the inhibition (*T*) or E_{max} threshold
400 but tended to underestimate rates below the threshold (Figure 4 b,c). There were no
401 differences between R^2 and RMSE between the *T* model and E_{max} model fits. This
402 suggested that use of the E_{max} model, which requires an additional parameter (E_{max}), was
403 not justified. To test this, we calculated the AIC for each fit (Table 3). The AIC takes
404 into account both the prediction performance and number of model parameters and the
405 best model is the one providing the lowest AIC (Burnham & Anderson 2003). There
406 were no differences between *T* and E_{max} model AICs for fits to any of the data sets from
407 the BWF experiments. So statistically, there was no justification to use the E_{max} model
408 since the addition of an extra parameter did not improve the model fit. Consequently, all
409 results presented in this report are for fits made with the *T* model.
410 The BWFs demonstrated that sensitivity of photosynthesis to inhibition by UVR was

not significantly different between cells grown under elevated and ambient CO_2. For *E. huxleyi* cultures grown in either condition, the average specific weights for inhibition of photosynthesis (ε [λ], [mW m^{-2}]$^{-1}$) were not significantly different over the full wavelength range (i.e. differences were less than the standard error of the average weight) (Figure 5). The overall shape of the BWF is a decrease in weights from 290 to 345 nm with an exponential slope of about 7% nm^{-1} and a relatively constant weight at longer wavelengths. The sensitivity to inhibition by PAR (ε_{PAR}, (W m^{-2})$^{-1}$) was low and also not significantly different between growth conditions (Table 4). At the average ε_{PAR}, PAR inhibition would only become significant (E^*_{inh} >1) at exposures > 300 W m^{-2} (ca 1290 µmol photons m^{-2} s^{-1}). The fitted parameters for both treatments using the *T* model for a 1 h incubation in the Photoinhibitron, i.e. the maximum rates of photosynthesis in the absence of inhibition, $P^B_{s,}$ the saturation irradiance parameter, E_s and the biological weight of inhibitory effect of PAR , showed higher values under elevated CO_2 conditions but the results were not significantly different than those observed under ambient CO_2 levels (Table 4).

Discussion

The results from this study show that *E. huxleyi* RCC 1226 is a highly calcifying strain with similar capability for assimilating organic and inorganic carbon as particulate material in the cell. The acclimation to elevated CO_2 levels in this strain over two weeks did not produce significant changes in the growth rates but increased organic carbon and nitrogen quotas. The fact that growth rates of *E. huxleyi* did not change under the CO_2 concentrations used in this experiment (Table 2) is contrary to that observed in another strain of this coccolithophore during mesocosm incubations, where elevated CO_2 clearly inhibited the growth rate compared to ambient CO_2 (Table 2, (Segovia et al. 2017)).

437 The strain in this mesocosm experiment has similar characteristics to the overcalcified
438 Type A strain isolated from the Norwegian Sea used for this study (Segovia et al. 2017).
439 However, the effects of elevated CO_2 levels on coccolithophores are sometimes
440 contradictory and not always significant as shown in recent meta-analyses (Kroeker et
441 al. 2013, Meyer & Riebesell 2015). Additionally, POC production and cell quota
442 significantly increased by 15% in cells acclimated to elevated CO_2 concentrations in
443 concordance with previous studies (Riebesell & Tortell 2011, Lorenzo et al. 2018).
444 Given the increased production and quotas of organic carbon and nitrogen for similar
445 growth rates, bigger cells might be expected under elevated CO_2 conditions, at least
446 regarding the size of the organic part of the cell (Aloisi 2015). Unfortunately, estimation
447 of cell size cannot be easily performed in this strain without taking into consideration
448 the carbonate coccosphere size, which can vary as a function of the number of layers of
449 coccoliths. Independent analysis of the coccolith metrics and coccosphere diameter in
450 our study showed that elevated CO_2 conditions resulted in smaller cells than under
451 ambient CO_2 conditions due to decreases in calcification. With this information it
452 remained unknown if the size of the organic part of the cell also changed with the
453 increase in CO_2.
454 The results based on the biometrics were in agreement with the decrease in PIC rates
455 under elevated CO_2 observed in our study using the microdiffusion technique (MDT.
456 (Paasche & Brubak 1994, Poulton et al. 2010). They are also in agreement with
457 previous studies that indicate a significant effect of elevated CO_2 in coccolithophores
458 calcification over production rates (Riebesell & Tortell 2011, Lorenzo et al. 2018).
459 Calcification rates observed in this strain are within the higher limit observed in cultures
460 (Balch et al. 2007) and similar to other *Emiliania* strains, such as the clone E88 isolated
461 from the Gulf of Maine (Balch et al. 1996, Balch et al. 1992). Despite good recovery
462 percentage and low variability, the MDT estimated rates of PIC production were

463 different from, and considerably higher than, mean daily rates predicted multiplying the
464 growth rate and inorganic carbon: chl quota. Balch et al. (1996) made a similar
465 calculation for a large set of continuous culture experiments with *E. huxleyi* and
466 observed that the predicted daily rate of calcification typically underestimated MDT
467 measurements by ~ 40%, which they attributed to temporal uncoupling between
468 photosynthesis and calcification. In other words, the partitioning of total photosynthetic
469 activity between inorganic and organic products can vary through the light period.
470 Similar to Balch et al. (1996), we found that predicted daily rate of total C incorporation
471 (POC +PIC) was closer to (~80%) the total MDT rate. The remaining discrepancy is
472 probably due to these experiments being conducted at different times in two different
473 labs.
474 De Bodt et al. (2010) proposed that the decrease in cellular PIC production rates at
475 elevated pCO_2 could produce a lower calcite content per coccolith, a decrease in
476 coccoliths number per cell or, a decrease in the coccolith production rate, these effects
477 not being mutually exclusive. Decreased calcification at lowered pH may be due to a
478 lower saturating state of calcite in the coccolith vesicles and subsequently disturbed
479 nucleation and formation of the crystallization (Zondervan et al. 2002). Recently,
480 Beaufort et al. (2011) demonstrated that the mass of the coccoliths decreased because of
481 a lower calcite content due to acidification. In the work presented here, the
482 morphometric analyses of coccoliths and coccospheres of *E. huxleyi* in both CO_2
483 conditions revealed that the coccosphere-sized particles showed a reduction trend with
484 increasing pCO_2 as already shown (De Bodt et al. 2010). The central area and the
485 number of slits were bigger under elevated CO_2, indicating less calcification under more
486 acidic conditions. Thus, the cells showed that the coccoliths and the coccospheres were
487 affected by elevated CO_2 concentrations although these alterations did not contribute to

increase the susceptibility of *E. huxleyi* to UVR, as opposed to studies describing an increase in inhibition of photosynthesis under the same scenario (Gao et al. 2009). The susceptibility of photosynthesis to UVR was estimated using biological weighting functions (BWFs) for the inhibition of photosynthesis, and a model that predicts primary productivity behaviour under PAR and UVR exposures. Among the different models tested, the *T* model provided the best prediction for inhibition of photosynthesis. Along with previous studies using the same model (Sobrino et al. 2005, Sobrino et al. 2009, Sobrino et al. 2008), these results suggest that there is an exposure threshold above which inhibition of photosynthesis is more severe because repair rate is limited. While inhibition is absent below this exposure threshold in the *T* model, more recent studies indicate that inhibition is still present but much less severe since repair rate increases with exposure (Neale et al. 2014). This below-threshold response is quantified in the E_{max} model through introduction of an additional parameter (Neale et al. 2014). Unfortunately, in the case of *E. huxleyi*, rates were too variable to resolve the below-threshold response. Therefore, the E_{max} and *T* models gave equivalent AIC values and the additional parameter was not justified. However, the *T* model tends to underestimate the maximum rate of uninhibited photosynthesis (P^B_s) since it ignores any inhibition below the threshold. For this reason, the E_{max} model is more appropriate for modelling primary productivity in the ocean (Neale et al. 2014). It could be also the reason why the *T* model P^B_s estimates were lower than the POC incorporation rates measured under culture conditions (no UV at saturating PAR). Further experiments should be performed with *E. huxleyi* to better define inhibition at lower exposures to enable fitting of the E_{max} model. Nevertheless, the results demonstrated that the *T* model provides a good basis for comparing responses to UV of *E. huxleyi* growing at different CO_2 concentrations. The results from this study demonstrate that photosynthesis in *E. huxleyi* under saturating light and nutrient conditions showed the same sensitivity to UVR exposure

514 under present atmospheric CO_2 levels (400 ppm) and elevated CO_2 levels predicted for
515 the end of the century (800 ppm) (IPCC 2014). The sensitivity of each phytoplankton
516 species to UVR is determined by the capability for protection and repair to counteract
517 UVR damage and the influence of the environmental factors on this capability in
518 different ways, increasing damage, decreasing efficiency of repair and indirectly
519 promoting repair and protection mechanisms (Litchman et al. 2002, Neale 2001). In
520 addition to the individual processes that take part in the development of these
521 mechanisms, the basal cell metabolism controls the degree of activity in the cell. The
522 fact that *E. huxleyi* showed the same sensitivity of photosynthesis to UVR in cells
523 grown both under ambient and under elevated CO_2 concentrations in our study is not
524 surprising, since the responses to UVR at increased CO_2 are diverse between different
525 taxa (Gao et al. 2009, Gao et al. 2012, García-Gómez et al. 2014, Sobrino et al. 2005,
526 Sobrino et al. 2009, Sobrino et al. 2008, Wu et al. 2012) and even between different
527 strains. One of the main questions is why there is such a variety of responses. Raven
528 (1991) proposed theoretically that a downregulation of the photosynthetic machinery in
529 phytoplankton under elevated CO_2 conditions could increase the resource use efficiency
530 and several experimental studies have supported this contention (García-Gómez et al.
531 2016, Sobrino et al. 2014). In *Thalassiosira pseudonana* and natural phytoplankton
532 assemblages the higher chlorophyll-specific photosynthesis observed under elevated
533 CO_2 levels was related to decreases in cellular chlorophyll content (Sobrino et al. 2009,
534 Sobrino et al. 2008). In addition, decreases in CCM activity, general enzymatic activity
535 and Rubisco content have been also observed under elevated CO_2 conditions (Wu et al.
536 2010, Sobrino et al. 2014). This suggests that elevated CO_2 might increase passive
537 diffusion rates and decrease the amount of energy and metabolites necessary to drive the
538 active transport of carbon to Rubisco, finally decreasing the whole cell metabolism.
539 This “downregulated” metabolism under elevated CO_2 acclimated conditions also has a

lower activation state of the general defence mechanism (Sobrino et al. 2014) which might affect the repair process of UVR-caused damage. A reduced amount or activity of the enzymes involved in the repair of the photosynthesis apparatus would increase the susceptibility to UVR. This results in more photoinhibition when UVR stress is imposed than the stress that would occur in cells with normal metabolic activity (Gao et al. 2009, Gao et al. 2012, Sobrino et al. 2009, Sobrino et al. 2014, Sobrino et al. 2008). In any case, it is expected that downregulation would decrease the catalytic costs of photosynthesis if growth is not energy limited by any metabolic demand (i.e. light, nutrients, etc), as it was in studies showing increases in sensitivity to UVR under enhanced CO_2 (Gao et al. 2009, Gao et al. 2012, Sobrino et al. 2009, Sobrino et al. 2014, Sobrino et al. 2008). Specific studies including calculations about the catalytic machinery costs under elevated CO_2 conditions are scarce (Raven et al. 2014). However, in this study *E. huxleyi* chl a content did not decrease at elevated CO_2, and growth rate, as a good indicator of the increased resource use efficiency under elevated CO_2 conditions neither showed significant increases. Hence, it appears that a full downregulation was not attained in this species, possibly because the energy savings due to less CCM activity were counterbalanced by the increased energy demand for other processes. In this case, a higher metabolic activity to compensate for the lower calcification rates due to increased CO_2 could be a major cause. Another possibility is that CCM downregulation under elevated CO_2 was not sufficient to induce the full downregulation of the cell metabolism. Supporting this last contention, Lorenzo et al (2018) determined the relative fraction of HCO_3^- and CO_2 uptake in a similar *E. huxleyi* strain during a natural bloom, by using the isotope disequilibrium assay (Martin & Tortell 2006), and found that HCO_3^- was the main C_i source for photosynthesis and was not affected by CO_2. As a consequence, if downregulation of cell metabolism did not occur, increases in sensitivity to UVR would not be expected.

566 Coccolithophores have been described as resistant to photoinhibition (Paasche 2001)
567 and it is suggested that the coccoliths could play photoprotective role in mitigating
568 excess PAR and UVR in *E. huxleyi* (Xu et al. 2016). These findings suggest that
569 coccolithophores may have an advantage compared to other phytoplankton groups
570 regarding stressful irradiance management (Raven & Crawfurd 2012). However, several
571 studies have demonstrated the sensitivity of *E. huxleyi* to solar UV exposure (Buma et
572 al. 2000, Gao et al. 2009, Guan & Gao 2010). In our study, cellular absorbance of UVR
573 and PAR was similar between ambient and elevated CO_2 concentrations and the
574 comparison with other published results showed that *E. huxleyi* has similar UV spectral
575 sensitivity as other phytoplankton species at ambient CO_2 concentration (Figure 6a).
576 This is further borne out by comparing the predicted response of different species to
577 average, midday summer irradiance at a temperate latitude (Table 5). In particular, the
578 sensitivity of *E. huxleyi* strain used for this study seems to be similar to the Chlorophyte
579 *Nannochloris atomus* and the diatom *T. pseudonana* at ambient CO_2. For cells
580 acclimated to elevated CO_2 concentrations, *E. huxleyi* and *N. atomus* also showed
581 similar susceptibility to UV (Figure 6b, Table 5). However, *Nannochloropsis gaditana*
582 at ambient CO_2 and *T. pseudonana* at elevated CO_2 are more sensitive than *E. huxleyi*,
583 reflecting the physiological differences discussed previously.
584
585 During the past years there is a growing body of studies focusing on the effects of ocean
586 acidification on coccolithophores (Riebesell & Tortell 2011). Our results analyzing the
587 role of UVR in combination with the increase in CO_2 contribute to this increasing
588 knowledge. They indicate that the sensitivity to UVR will be the same at elevated as
589 ambient CO_2 conditions in this strain of *E. huxleyi*. Sensitivity to UV may not have
590 varied in this strain because energy savings due to less CCM activity was used to satisfy
591 the increased energy demands for other processes such as PIC production, or because

CCM activity was not significantly affected by CO_2. Our results also show that future scenarios of global change, characterized by elevated CO_2 atmospheric concentrations, might promote carbon fixation as organic matter by this calcifying *E. huxleyi* strain. However, a similar proportion of inorganic carbon fixation will be inhibited by the ocean acidification, counterbalancing the positive effect observed on primary production. The net response results in a neutral effect of ocean acidification on this strain of *E. huxleyi* regarding growth rate, carbon fixation and photosynthesis inhibition by UVR under elevated CO_2 conditions.

Acknowledgments

This work was funded by CTM/MAR 2010-17216 research grant from the Spanish Ministry for Science and Innovation (Spain) to MS. MRL was funded by a FPU grant from the Ministry for Education and by a grant from the University of Malaga (Plan Propio) (Spain) to carry out a short-stay at PJN laboratory. We are grateful to Kevin Mackenzie and staff from the Microscopy Unit at the Institute of Medical Sciences, University of Aberdeen (UK).

Bibliography:

Aloisi, G. 2015. Covariation of metabolic rates and cell size in coccolithophores. *Biogeosciences* 12:4665-92.

Bach, L. T., Bauke, C., Meier, K. J. S., Riebesell, U. & Schulz, K. G. 2012. Influence of changing carbonate chemistry on morphology and weight of coccoliths formed by *Emiliania huxleyi*. *Biogeosciences* 9:3449-63.

Bais, A. F., Lucas, R. M., Bornman, J. F., Williamson, C. E., Sulzberger, B., Austin, A. T., Wilson, S. R., Andrady, A. L., Bernhard, G., McKenzie, R. L., Aucamp, P. J.,

617 Madronich, S., Neale, R. E., Yazar, S., Young, A. R., de Gruijl, F. R., Norval, M.,
618 Takizawa, Y., Barnes, P. W., Robson, T. M., Robinson, S. A., Ballare, C. L., Flint, S.
619 D., Neale, P. J., Hylander, S., Rose, K. C., Wangberg, S. A., Hader, D. P., Worrest, R.
620 C., Zepp, R. G., Paul, N. D., Cory, R. M., Solomon, K. R., Longstreth, J., Pandey, K.
621 K., Redhwi, H. H., Torikai, A. & Heikkila, A. M. 2018. Environmental effects of ozone
622 depletion, UV radiation and interactions with climate change: UNEP Environmental
623 Effects Assessment Panel, update 2017. *Photochem. Photobio. Sci.* 17:127-79.

624 Bais, A. F., McKenzie, R. L., Bernhard, G., Aucamp, P. J., Ilyas, M., Madronich, S. &
625 Tourpali, K. 2015. Ozone depletion and climate change: impacts on UV radiation.
626 *Photochem. Photobio. Sci.* 14:19-52.

627 Balch, W., Drapeau, D., Bowler, B. & Booth, E. 2007. Prediction of pelagic
628 calcification rates using satellite measurements. *Deep Sea Res. II Top. Stud. Oceanogr.*
629 54:478-95.

630 Balch, W. M., Fritz, J. & Fernandez, E. 1996. Decoupling of calcification and
631 photosynthesis in the coccolithophore *Emiliania huxleyi* under steady-state light-limited
632 growth. *Mar. Ecol. Prog. Ser.* 142:87-97.

633 Balch, W. M., Holligan, P. M. & Kilpatrick, K. A. 1992. Calcification, photosynthesis
634 and growth of the bloom-forming coccolithophore, *Emiliania huxleyi*. *Cont. Shelf Res.*
635 12:1353-74.

636 Beardall, J., Sobrino, C. & Stojkovic, S. 2009. Interactions between the impacts of
637 ultraviolet radiation, elevated CO2, and nutrient limitation on marine primary
638 producers. *Photochem. Photobio. Sci.* 8:1257-65.

639 Beardall, J., Stojkovic, S. & Gao, K. 2014. Interactive effects of nutrient supply and
640 other environmental factors on the sensitivity of marine primary producers to ultraviolet
641 radiation: implications for the impacts of global change. *Aquatic Biol.* 22:5-23.

642 Beaufort, L., Probert, I., de Garidel-Thoron, T., Bendif, E. M., Ruiz-Pino, D., Metzl, N.,
643 Goyet, C., Buchet, N., Coupel, P., Grelaud, M., Rost, B., Rickaby, R. E. M. & de
644 Vargas, C. 2011. Sensitivity of coccolithophores to carbonate chemistry and ocean
645 acidification. *Nature* 476:80.

646 Boyd, P. W. & Doney, S. C. 2002. Modelling regional responses by marine pelagic
647 ecosystems to global climate change. *Geophys. Res. Lett.* 29:53-1-53-4.

648 Boyd, P. W. & Hutchins, D. A. 2012. Understanding the responses of ocean biota to a
649 complex matrix of cumulative anthropogenic change. *Mar. Ecol. Prog. Ser.* 470:125-35.

650 Brown, P. R., Lees, J. A. & Young, J. R. 2004. Calcareous nannoplankton evolution and
651 diversity through time. *In*: Thierstein, H. R. & Young, J. R. [Eds.] *Coccolithophores :*
652 *from molecular processes to global impact.* Springer, Berlin, pp. 481-508.

653 Buma, A. G. J., Van Oijen, T., Van De Poll, W., Veldhuis, M. J. W. & Gieskes, W. W.
654 C. 2000. The sensitivity of *Emiliania huxleyi* (Prymnesiophyceae) to ultraviolet-b
655 radiation. *J. Phycol.* 36:296-303.

656 Burnham, K. P. & Anderson, D. R. 2003. *Model Selection and Multimodel Inference: A*
657 *Practical Information-Theoretic Approach.* Springer Science & Business Media, 488.

658 Cleveland, J. S. & Weidemann, A. D. 1993. Quantifying absorption by aquatic
659 particles: A multiple scattering correction for glass fiber filters. *Limnol. Oceanogr.*
660 38:1321-27.

661 Cullen, J. J. & Neale, P. J. 1997. Biological weighting functions for describing the
662 effects of ultraviolet radiation on aquatic systems. *In*: Häder, D.-P. [Ed.] *Effects of*
663 *ozone depletion on aquatic ecosystems.* R. G. Landes, Austin, pp. 97-118.

664 Cullen, J. J., Neale, P. J. & Lesser, M. P. 1992. Biological weighting function for the
665 inhibition of phytoplankton photosynthesis by ultraviolet radiation. *Science* 258:646-50.

666 De Bodt, C., Van Oostende, N., Harlay, J., Sabbe, K. & Chou, L. 2010. Individual and
667 interacting effects of CO_2 and temperature on *Emiliania huxleyi* calcification: study of
668 the calcite production, the coccolith morphology and the coccosphere size.
669 *Biogeosciences* 7:1401-12.

670 Doney, S. C., Fabry, V. J., Feely, R. A. & Kleypas, J. A. 2009. Ocean Acidification:
671 The Other CO_2 Problem. *Annu. Rev. Mar. Sci.* 1:169-92.

672 Field, C. B., Behrenfeld, M. J., Randerson, J. T. & Falkowski, P. 1998. Primary
673 Production of the Biosphere: Integrating Terrestrial and Oceanic Components. *Science*
674 281:237.

675 Folt, C. L., Chen, C. Y., Moore, M. V. & Burnaford, J. 1999. Synergism and
676 antagonism among multiple stressors *Limnol. Oceanogr.* 44:864-77.

677 Gao, K., Ruan, Z., Villafañe, V. E., Gattuso, J.-P. & Helbling, E. W. 2009. Ocean
678 acidification exacerbates the effect of UV radiation on the calcifying phytoplankter
679 *Emiliania huxleyi*. *Limnol. Oceanogr.* 54:1855-62.

680 Gao, K., Xu, J., Gao, G., Li, Y., Hutchins, D. A., Huang, B., Wang, L., Zheng, Y., Jin,
681 P., Cai, X., Häder, D.-P., Li, W., Xu, K., Liu, N. & Riebesell, U. 2012. Rising CO_2 and
682 increased light exposure synergistically reduce marine primary productivity. *Nature*
683 *Climate Change* 2:519.

García-Gómez, C., Gordillo, F. J. L., Palma, A., Lorenzo, M. R. & Segovia, M. 2014. Elevated CO_2 alleviates high PAR and UV stress in the unicellular chlorophyte *Dunaliella tertiolecta*. *Photochem. Photobio. Sci.* 13:1347-58.

García-Gómez, C., Mata, M. T., Breusegem, F. V. & Segovia, M. 2016. Low-steady-state metabolism induced by elevated CO_2 increases resilience to UV radiation in the unicellular green-algae *Dunaliella tertiolecta*. *Environ. Exp. Bot.* 132:163-74.

Genty, B., Briantais, J. M. & Baker, N. 1989. The relationship between the quantum yield of photosynthetic electron transport and quenching of chlorophyll fluorescence. *Biochimica et Biophysica Acta* 990:87-92.

Guan, W. & Gao, K. 2010. Impacts of UV radiation on photosynthesis and growth of the coccolithophore *Emiliania huxleyi* (Haptophyceae). *Environ. Exp. Bot.* 67:502-08.

Guillard, R. R. L. & Ryther, J. H. 1962. Studies of marine plankton diatoms I. *Cyclotella nana* Hustedt, and *Detonula confervacea* (Cleve) Gran. *Can. J. Microbiology.* 8:229-39.

Häder, D.-P. 2011. Does Enhanced Solar UV-B Radiation Affect Marine Primary Producers in Their Natural Habitats? *Photochem. Photobiol.* 87:263-66.

Hoffmann, L. J., Breitbarth, E., Boyd, P. W. & Hunter, K. A. 2012. Influence of ocean warming and acidification on trace metal biogeochemistry. *Mar. Ecol. Prog. Ser.* 470:191-205.

Holligan, P. M., Fernández, E., Aiken, J., Balch, W. M., Boyd, P., Burkill, P. H., Finch, M., Groom, S. B., Malin, G., Muller, K., Purdie, D. A., Robinson, C., Trees, C. C., Turner, S. M. & van der Wal, P. 1993. A biogeochemical study of the coccolithophore, *Emiliania huxleyi*, in the North Atlantic. *Global Biogeochemical Cycl.* 7:879-900.

IPCC 2014. Climate Change 2014: Synthesis Report. Contribution of Working Groups I, II and III to the Fifth Assessment Report of the Intergovernmental Panel on Climate Change *In*: Team, C. W., Pachauri, R. K. & Meyer, L. A. [Eds.]. Geneva, Switzerland, pp. 151.

Kroeker, K. J., Kordas, R. L., Crim, R., Hendriks, I. E., Ramajo, L., Singh, G. S., Duarte, C. M. & Gattuso, J.-P. 2013. Impacts of ocean acidification on marine organisms: quantifying sensitivities and interaction with warming. *Global Change Biol.* 19:1884-96.

Litchman, E., Neale, P. J. & Banaszak, A. T. 2002. Increased sensitivity to ultraviolet radiation in nitrogen-limited dinoflagellates: photoprotection and repair. *Limnol. Oceanogr.* 47:86-94.

Lorenzo, M. R., Iñiguez, C., Egge, J. K., Larsen, A., Berger, S. A., García-Gómez, C. & Segovia, M. 2018. Increased CO_2 and iron availability effects on carbon assimilation and calcification on the formation of *Emiliania huxleyi* blooms in a coastal phytoplankton community. *Environ. Exp. Bot.* 148:47-58.

Mackey, K. R. M., Morris, J. J., Morel, F. M. M. & Kranz, S. A. 2015. Response of Photosynthesis to Ocean Acidification. *Oceanography* 28:74-91.

Martin, C. L. & Tortell, P. D. 2006. Bicarbonate transport and extracellular carbonic anhydrase activity in Bering Sea phytoplankton assemblages: Results from isotope disequilibrium experiments. *Limnol. Oceanogr.* 51:2111-21.

Meyer, J. & Riebesell, U. 2015. Reviews and Syntheses: Responses of coccolithophores to ocean acidification: a meta-analysis. *Biogeosciences* 12:1671-82.

729 Neale, P. J. 2000. Spectral weighting functions for quantifying the effects of ultraviolet
730 radiation in marine ecosystems. *In*: de Mora, S. J., Demers, S. & Vernet, M. [Eds.] *The*
731 *effects of UV radiation in the marine environment.* Cambridge Univ. Press, Cambridge,
732 pp. 72-100.

733 Neale, P. J. 2001. Effects of ultraviolet radiation on estuarine phytoplankton production:
734 Impact of variations in exposure and sensitivity to inhibition. *J. Photochem. Photobiol.*
735 *B* 62:1-8.

736 Neale, P. J. & Fritz, J. J. 2001. Experimental exposure of plankton suspensions to
737 polychromatic ultraviolet radiation for determination of spectral weighting functions.
738 *In*: Slusser, J., Herman, J. R. & Gao, W. [Eds.] *Ultraviolet Ground- and Space-based*
739 *Measurements, Models, and Effects.* SPIE-The International Society for Optical
740 Engineering, San Diego, pp. 291-96.

741 Neale, P. J., Pritchard, A. L. & Ihnacik, R. 2014. UV effects on the primary productivity
742 of picophytoplankton: biological weighting functions and exposure response curves of
743 *Synechococcus*. *Biogeosciences* 11:2883-95.

744 Neale, P. J. & Smyth, R. L. 2018. Are Warmer Waters, Brighter Waters? An
745 Examination of the Irradiance Environment of Lakes and Oceans in a Changing
746 Climate. *In*: Hader, D. P. & Gao, K. [Eds.] *Aquatic Ecosystems in a Changing Climate.*
747 CRC, pp. 89-115.

748 Paasche, E. 2001. A review of the coccolithophorid *Emiliania huxleyi*
749 (Prymnesiophyceae), with particular reference to growth, coccolith formation, and
750 calcification-photosynthesis interactions. *Phycologia* 40:503-29.

751 Paasche, E. & Brubak, S. 1994. Enhanced calcification in the coccolithophorid
752 *Emiliania huxleyi* (Haptophyceae) under phosphorus limitation. *Phycologia* 33:324-30.

753 Polovina, J. J., Howell, E. A. & Abecassis, M. 2008. Ocean's least productive waters are
754 expanding. *Geophys. Res. Lett.* 35.

755 Poulton, A. J., Charalampopoulou, A., Young, J. R., Tarran, G. A., Lucas, M. I. &
756 Quartlya, G. D. 2010. Coccolithophore dynamics in non-bloom conditions during late
757 summer in the central Iceland Basin (July-August 2007). *Limnol. Oceanogr.* 55:1601-
758 13.

759 Raven, J. A. 1991. Physiology of inorganic C acquisition and implications for resource
760 use efficiency by marine phytoplankton: relation to increased CO_2 and temperature.
761 *Plant, Cell Environ.* 14:779-94.

762 Raven, J. A., Beardall, J. & Giordano, M. 2014. Energy costs of carbon dioxide
763 concentrating mechanisms in aquatic organisms. *Photosynthesis Res.* 121:111-24.

764 Raven, J. A. & Crawfurd, K. 2012. Environmental controls on coccolithophore
765 calcification. *Mar. Ecol. Prog. Ser.* 470:137-66.

766 Riebesell, U. & Tortell, P. D. 2011. Effects of ocean acidification on pelagic organisms
767 and ecosystems. *In*: Gattuso, J.-P. & Lansson, L. [Eds.] *Ocean Acidification.* Oxford
768 University Press, Oxford, pp. 99-121.

769 Rost, B. & Riebesell, U. 2004. Coccolithophores and the biological pump: responses to
770 environmental changes. *In*: Thierstein, H. R. & Young, J. R. [Eds.] *Coccolithophores :*
771 *from molecular processes to global impact.* Springer, Berlin, pp. 99-125.

772 Segovia, M., Lorenzo, M. R., Maldonado, M. T., Larsen, A., Berger, S. A., Tsagaraki,
773 T. M., Lázaro, F. J., Iñiguez, C., García-Gómez, C., Palma, A., Mausz, M. A., Gordillo,
774 F. J. L., Fernández, J. A., Ray, J. L. & Egge, J. K. 2017. Iron availability modulates the
775 effects of future CO_2 levels within the marine planktonic food web. *Mar. Ecol. Prog.*
776 *Ser.* 565:17-33.

777 Shanklin, J. 2010. Reflections on the ozone hole. *Nature* 465:34.

778 Smyth, R. L., Sobrino, C., Phillips-Kress, J., Kim, H.-C. & Neale, P. J. 2012.
779 Phytoplankton photosynthetic response to solar ultraviolet irradiance in the Ross Sea
780 Polynya: Development and evaluation of a time-dependent model with limited repair.
781 *Limnol. Oceanogr.* 57:1602–18.

782 Sobrino, C., Neale, P. J. & Lubian, L. 2005. Interaction of UV-Radiation and Inorganic
783 Carbon Supply in the Inhibition of Photosynthesis: Spectral and Temporal Responses of
784 Two Marine Picoplankters. *Photochem. Photobiol.* 81:384–93.

785 Sobrino, C., Neale, P. J., Phillips-Kress, J. D., Moeller, R. E. & Porter, J. 2009.
786 Elevated CO_2 increases sensitivity to ultraviolet radiation in lacustrine phytoplankton
787 assemblages. *Limnol. Oceanogr.* 54:2448-59.

788 Sobrino, C., Segovia, M., Neale, P. J., Mercado, J. M., García-Gómez, C., Kulk, G.,
789 Lorenzo, M. R., Camarena, T., van de Poll, W. H., Spilling, K. & Ruan, Z. 2014. Effect
790 of CO_2, nutrients and light on coastal plankton. IV. Physiological responses. *Aquatic*
791 *Biol.* 22:77-93.

792 Sobrino, C., Ward, M. L. & Neale, P. J. 2008. Acclimation to elevated carbon dioxide
793 and ultraviolet radiation in the diatom *Thalassiosira pseudonana*: Effects on growth,

794 photosynthesis, and spectral sensitivity of photoinhibition. *Limnol. Oceanogr.* 53:494-
795 505.

796 Somavilla, R., González-Pola, C. & Fernández-Diaz, J. 2017. The warmer the ocean
797 surface, the shallower the mixed layer. How much of this is true? *Journal of*
798 *Geophysical Research: Oceans* 122:7698-716.

799 Triantaphyllou, M., Dimiza, M., Krasakopoulou, E., Malinverno, E., Lianou, V. &
800 Souvermezoglou, E. 2010. Seasonal variation in *Emiliania huxleyi* coccolith
801 morphology and calcification in the Aegean Sea (Eastern Mediterranean). *Geobios*
802 43:99-110.

803 Tzortziou, M. 2004. *Measurements and Characterization of Optical Properties in the*
804 *Chesapeake Bay's Estuarine Waters Using In-Situ Measurements, Modis Satellite*
805 *Observations, and Radiative Transfer Modeling.* University of Maryland.

806 Weatherhead, E. C. & Andersen, S. B. 2006. The search for signs of recovery of the
807 ozone layer. *Nature* 441:39-45.

808 Wu, X., Gao, G., Giordano, M. & Gao, K. 2012. Growth and photosynthesis of a diatom
809 grown under elevated CO_2 in the presence of solar UV radiation. *Fundam. Appl.*
810 *Limnol.* 180:279-90(12).

811 Wu, Y., Gao, K. & Riebesell, U. 2010. CO_2-induced seawater acidification affects
812 physiological performance of the marine diatom *Phaeodactylum tricornutum*.
813 *Biogeosciences* 7:2915-23.

814 Young, J. R., Geisen, M. & Probert, I. 2005. A review of selected aspects of
815 coccolithophore biology with implications for paleobiodiversity estimation.
816 *Micropaleontology* 51:267-88.

817 Zeebe, R. E. & Wolf-Gladrow, D. 2001. *CO_2 in Seawater: Equilibrium, Kinetics,*
818 *Isotopes.* Elsevier, 360.

819 Zondervan, I., Rost, B. & Riebesell, U. 2002. Effect of CO_2 concentration on the
820 PIC/POC ratio in the coccolithophore *Emiliania huxleyi* grown under light-limiting
821 conditions and different daylengths. *J. Exp. Mar. Biol. Ecol.* 272:55-70.
822
823

824 **Table 1.** Cellular characteristics of *Emiliania huxleyi* grown under ambient CO_2 (400
825 ppm) and elevated CO_2 (800 ppm). Mean ± standard deviation (n=3-4 independent
826 cultures). Statistically significant differences ($p < 0.05$) are indicated with an asterisk
827 (*).

	Ambient CO_2	**Elevated** CO_2
Specific growth rate (d^{-1})	0.60 ± 0.06	0.58 ± 0.03
POC quota (µg µg Chl a^{-1})	57.7 ± 0.38*	68.0 ± 0.89*
PIC quota (µg µg Chl a^{-1})	21.27 ± 1.35	22.55 ± 1.83
PON quota (µg µg Chl a^{-1})	9.93 ± 0.24*	10.56 ± 0.30*
PIC:POC (mol mol^{-1})	0.37 ± 0.02	0.33 ± 0.03
POC:PON (mol mol^{-1})	7.48 ± 0.22*	8.17 ± 0.31*
Chl-*a* quota (pg $cell^{-1}$)	0.23 ± 0.04	0.25 ± 0.05

828

829

Table 2. Morphometric analysis of detached coccoliths and coccospheres of *Emiliania huxleyi* grown under ambient CO_2 (400 ppm) and elevated CO_2 (800 ppm). Mean ± standard deviation (µm). Statistically significant differences ($p < 0.05$) are indicated with an asterisk. Measured parameters on coccoliths DSL: distal shield length; DSW: distal shield width; DSA: distal shield area; CAL: central area length; CAW: central area width and OSL: outer shield length.

	Ambient CO_2	**Elevated** CO_2
Coccoliths		
DSL	3.17 ± 0.27	3.17 ± 0.28
DSW	2.54 ± 0.27	2.55 ± 0.33
DSA	6.39 ± 1.21	6.40 ± 1.28
CAL	1.42 ± 0.20	1.48 ± 0.19
CAW	0.83 ± 0.14*	0.94 ± 0.17*
OSL	0.87 ± 0.11	0.83 ± 0.09
Number of slits	30.72 ± 3.40*	34.16 ± 3.37*
n	30	30
Coccospheres		
Length	6.88 ± 0.52*	6.44 ± 0.61*
Width	6.47 ± 0.47	6.22 ± 0.59

n	25	30

836

837

838 **Table 3.** Difference in the Akaike Information Criterion (AIC) calculated for fits using
839 E vs T and T vs E_{max} exposure response models to experimental data on the response of
840 *Emiliania huxleyi* photosynthesis to UV + PAR exposure. Positive values indicate
841 improvement (lowering) of the AIC (Burnham & Anderson 2003). Listed is the
842 average±standard deviation (SD) difference for n=6 sets of experimental data.

843

	ΔAIC	
	(*E vs. T*)	**(*T vs. E_{max}*)**
Average	101.7	-0.01
SD	15.5	0.71

844

845

Table 4. Fitted parameters for the BWF-PI model of photosynthesis by *Emiliania huxleyi* using the *T* exposure response model. Listed are the light saturated rates of photosynthesis in the absence of inhibition (P^B_s, µg C µg Chl a^{-1}), characteristic irradiances for light saturation (E_s,W m^{-2}, PAR) and coefficients for inhibition by PAR (ε_{PAR}, $(W\ m^{-2})^{-1}$), mean ± standard errors for n ≥ 3 experiments under each condition ambient (400 ppm) and elevated (800 ppm) CO_2 concentration.

	Ambient CO_2	**Elevated** CO_2
P^B_s	2.17 ± 0.22	2.20 ± 0.21
E_s	13.7±0.84	14.5 ± 1.03
ε_{PAR} x 10^{-3}	3.26±0.33	3.41 ± 0.27

854 **Table 5**. Weighted irradiance values (E^*_{inh}) and % inhibition of photosynthesis
855 estimated using the T-model BWF/P-E for different phytoplankton species grown
856 under ambient (400 ppm) or elevated CO_2 (800 ppm) (cf. Figure 8). Response is based
857 on average, midday summer spectral irradiance at a temperate location (39°N) as
858 recorded at the Smithsonian Environmental Research Center (Neale 2001).

	E^*_{inh}		% Inhibition	
Species	Ambient CO_2	Elevated CO_2	Ambient CO_2	Elevated CO_2
Emiliania huxleyi	3.74	3.81	0.73	0.74
Nannochloris atomus[1]	4.15	4.05	0.76	0.75
Nannochloropsis gaditana[1]	5.02	4.18	0.80	0.76
Thalassiosira pseudonana[2]	3.17	5.20	0.68	0.81

859

860 [1]Using BWF/P-E results from Sobrino et al. (2005)

861 [2]Using BWF/P-E results for cultures grown under PAR irradiance as reported by
862 Sobrino et al. (2008)

863

Figure Legends

Figure 1. Cellular absorbance of UVR and PAR measured as Chl *a* specific absorption (a*[λ] m^2 mg $Chla^{-1}$) of *Emiliania huxleyi* under ambient (400 ppm) and elevated CO_2 (800 ppm) concentrations (n=3). The solid line corresponds to cultures grown under ambient CO_2 concentration and the dashed line corresponds to elevated CO_2 cultures.

Figure 2. Production rates of *Emiliania huxleyi* under ambient (400 ppm, solid) and elevated (800 ppm, open) CO_2 during growth as measured using the microdiffusion technique. (a) particulate inorganic carbon (PIC), (b) particulate organic carbon (POC) and, (c) PIC: POC productivity ratio. Bars represent the mean of triplicate cultures and the error bars denote the standard deviation. Differences are statistically significant at p=0.002 (a) or p<0.001 (b,c).

Figure 3. Average rates of photosynthesis *vs.* PAR irradiance (W m^{-2}) for *Emiliania huxleyi* cultures (n=3) grown under ambient (400 ppm, solid symbols) or high (800 ppm, open symbols) CO_2 for the 12 different spectral treatments (specified in Supplemental Table S1) in the photoinhibitron with 10 irradiance levels within each treatment. Panel titles identify the lower (cut-off) wavelength of each irradiance treatment specifying the wavelengths of 1% and 50% transmission (respectively). Panels are ordered from shortest to longest cut-off wavelengths. Further details on spectral treatments are listed by panel letter in Supplemental Table S1. Due to variation within the Xe-lamp beam, spectral composition within treatment varies resulting in some scatter in the P-E relationship (i.e. values around 75 W m^{-2} in plot F). This spectral variation is accounted for in the model fit.

Figure 4. The panels illustrate the observed (points) vs. fitted (lines) results for three BWF/P-E models, the E (a), T (b) and E_{max} (c) models (see materials and methods for definition of models). Biomass-specific photosynthesis (µgC µg chl $a^{-1}h^{-1}$) plotted as a function of UV+PAR exposure weighted by a spectral biological weighting function for

890 inhibition, E^*_{inh}(dimensionless). E^*_{inh} reflects the varying inhibition effectiveness of the
891 exposure conditions (i.e. one of the 10 irradiance levels of the 12 different spectral
892 treatments as described in Table S1) corresponding to each of the measured
893 photosynthetic rates (Figure 3). Root mean square error (RMSE) of the fitted model is
894 in µg C µg chl $a^{-1}h^{-1}$.
895 **Figure 5.** BWFs for the inhibition of photosynthesis by UVR (ε [λ], [mW m^{-2}]$^{-1}$) of
896 *Emiliania huxleyi* cultures under present atmospheric (400 ppm, solid line) and elevated
897 (800 ppm, dashed line) CO_2. Curves are the average BWF (n=3-4) for each treatment.
898 The thin and thick line error bars show representative standard errors of the mean
899 (SEM) for the average BWF of ambient and elevated CO_2 cultures, respectively,
900 calculated from the standard error estimates of the individual BWFs.
901 **Figure 6.** Biological weighting functions for the inhibition of photosynthesis by UV ((ε
902 [λ], [mW m^{-2}]$^{-1}$) estimated by statistical analysis of data from different phytoplankton
903 species. The solid line is the average biological weight for *Thalassiosira pseudonana*
904 (Sobrino et al 2008), the short dashed line is for *Nannochloris atomus* (Sobrino et al
905 2005), the dotted line is for *Nannochloropsis gaditana* (Sobrino et al 2005), and the
906 long dashed line is *Emiliania huxleyi*, at ambient (400 ppm) (a) and elevated (800 ppm)
907 (b) CO_2 conditions. The error bars show representative standard errors.
908
909
910
911

Figure 1. Cellular absorbance of UVR and PAR measured as Chl *a* specific absorption (a*[λ] m^2 mg $Chla^{-1}$) of *Emiliania huxleyi* under ambient (400 ppm) and elevated CO_2 (800 ppm) concentrations (mean±std. dev., n=3). The solid line corresponds to cultures grown under ambient CO_2 concentration and the dashed line corresponds to elevated CO_2 cultures.

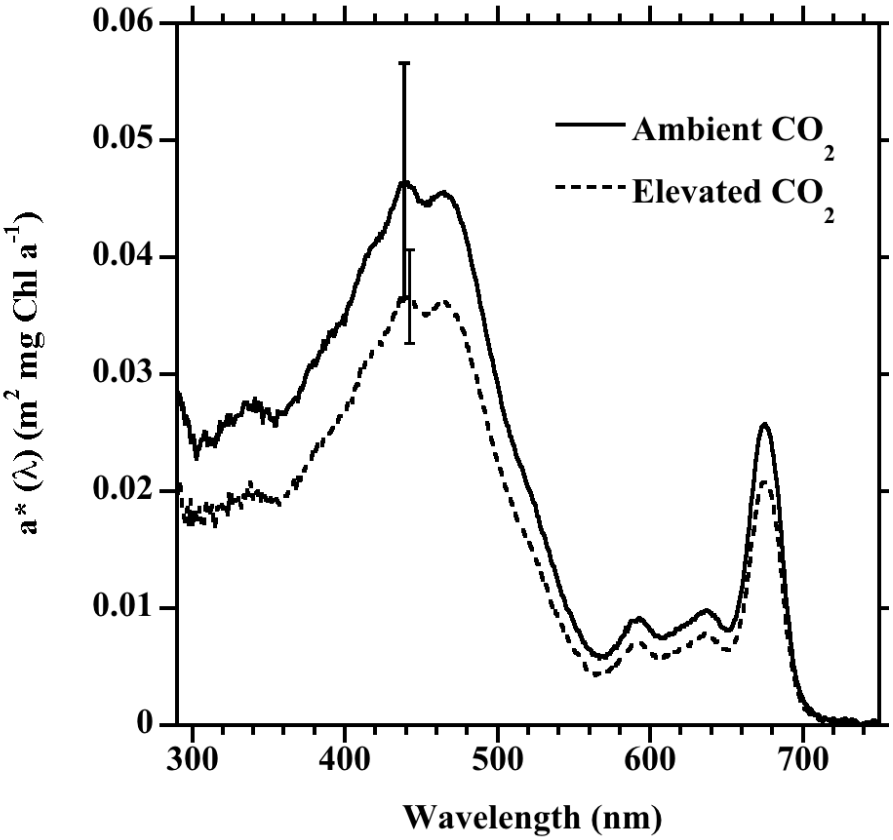

Figure 2. Production rates of *Emiliania huxleyi* under ambient (400 ppm, solid) and elevated (800 ppm, open) CO_2 during growth as measured using the microdiffusion technique. (a) particulate inorganic carbon (PIC), (b) particulate organic carbon (POC) and, (c) PIC: POC productivity ratio. Bars represent the mean of triplicate cultures and the error bars denote the standard deviation. Differences are statistically significant at p=0.002 (a) or p<0.001 (b,c).

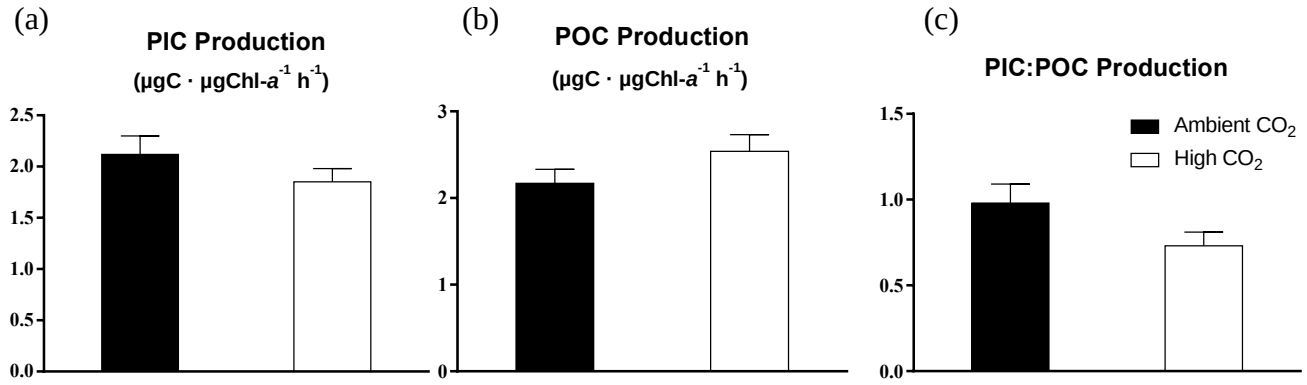

Figure 3. Average rates of photosynthesis *vs.* PAR irradiance (W m^{-2}) for *Emiliania huxleyi* cultures (n=3) grown under ambient (400 ppm, solid symbols) or high (800 ppm, open symbols) CO_2 for the 12 different spectral treatments (specified in Supplemental Table S1) in the photoinhibitron with 10 irradiance levels within each treatment. Panel titles identify the lower (cut-off) wavelength of each irradiance treatment specifying the wavelengths of 1% and 50% transmission (respectively). Panels are ordered from shortest to longest cut-off wavelengths. Further details on spectral treatments are listed by panel letter in Supplemental Table S1. Due to variation within the Xe-lamp beam, spectral composition within treatment varies resulting in some scatter in the P-E relationship (i.e. values around 75 W m^{-2} in plot F). This spectral variation is accounted for in the model fit.

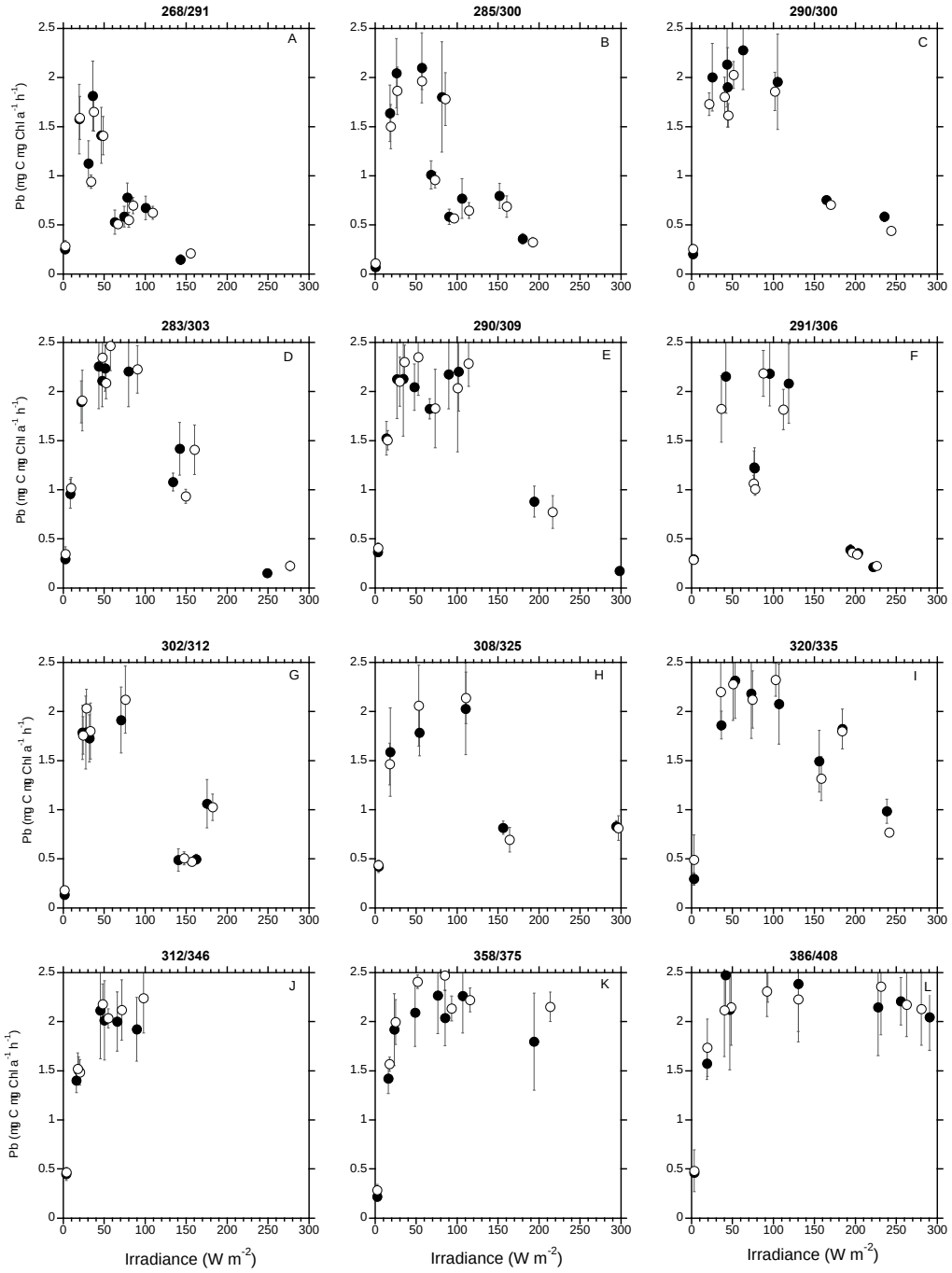

Figure 4. The panels illustrate the observed (points) vs. fitted (lines) results for three BWF/P-E models, the *E* (a), *T* (b) and E_{max} (c) models (see materials and methods for definition of models). Biomass-specific photosynthesis (µg C µg chl $a^{-1}h^{-1}$) plotted as a function of UV+PAR exposure weighted by a spectral biological weighting function for inhibition, E^*_{inh}(dimensionless). E^*_{inh} reflects the varying inhibition effectiveness of the exposure conditions (i.e. one of the 10 irradiance levels of the 12 different spectral treatments as described in Table S1) corresponding to each of the measured photosynthetic rates (Figure 3). Root mean square error (RMSE) of the fitted model is in µg C µg Chl $a^{-1}h^{-1}$.

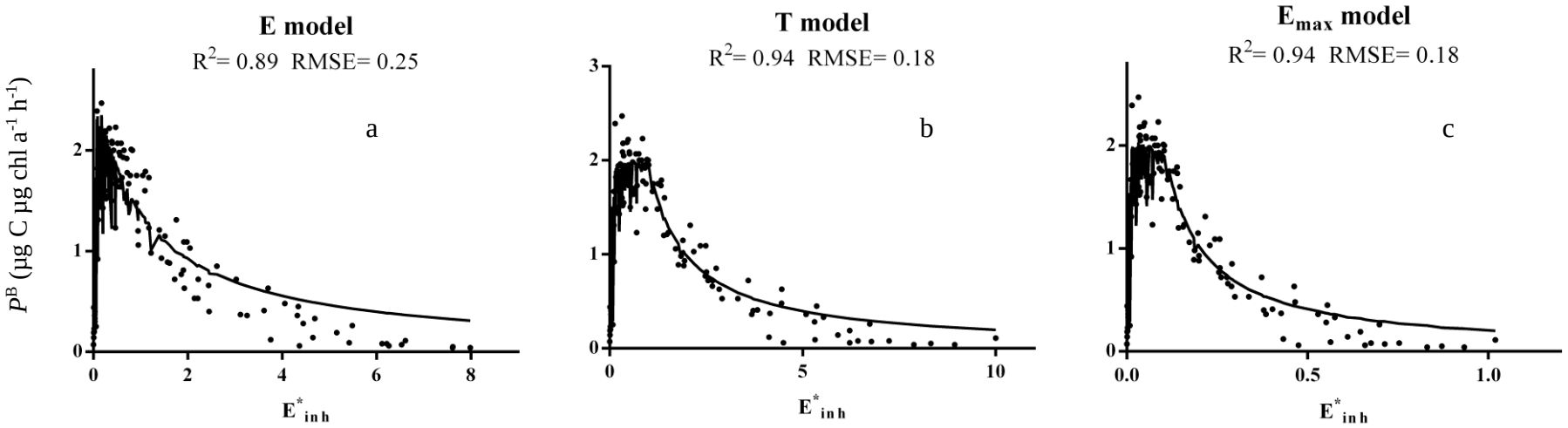

Figure 5. BWFs for the inhibition of photosynthesis by UVR (ε [λ], [mW m^{-2}]$^{-1}$) of *Emiliania huxleyi* cultures under present atmospheric (400 ppm, solid line) and elevated (800 ppm, dashed line) CO_2. Curves are the average BWF (n=3-4) for each treatment. The thin and thick line error bars show representative standard errors of the mean (SEM) for the average BWF of ambient and elevated CO_2 cultures, respectively, calculated from the standard error estimate of the individual BWFs.

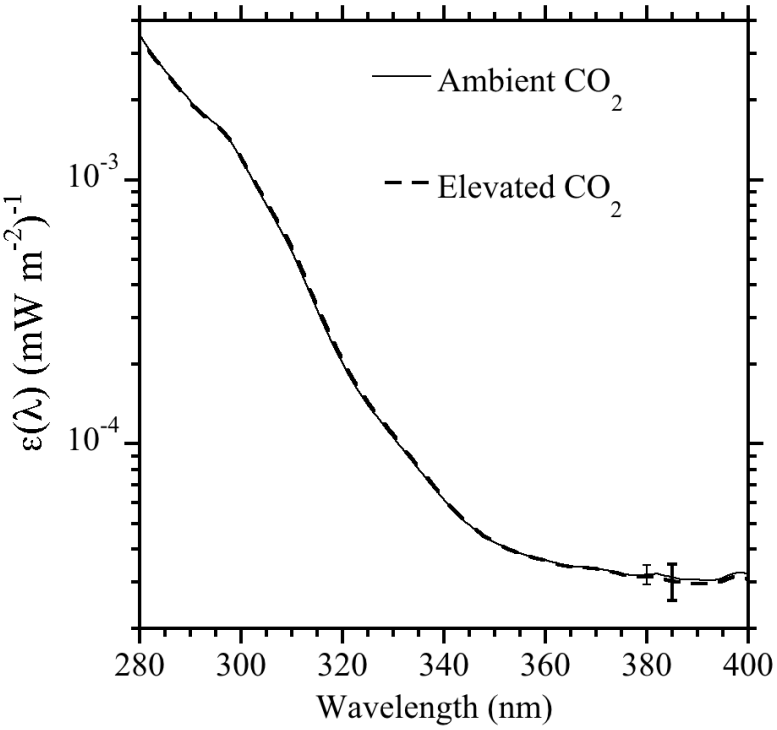

962 **Figure 6.** Biological weighting functions for the inhibition of photosynthesis by UV ((ε
963 [λ], [mW m^{-2}]$^{-1}$) estimated by statistical analysis of data from different phytoplankton
964 species. The solid line is the average biological weight for *Thalassiosira pseudonana*
965 (Sobrino et al 2008), the short dashed line is for *Nannochloris atomus* (Sobrino et al
966 2005), the dotted line is for *Nannochloropsis gaditana* (Sobrino et al 2005), and the
967 long dashed line is *Emiliania huxleyi*, at ambient (400 ppm) (a) and elevated (800 ppm)
968 (b) CO_2 conditions. The error bars show representative standard errors.

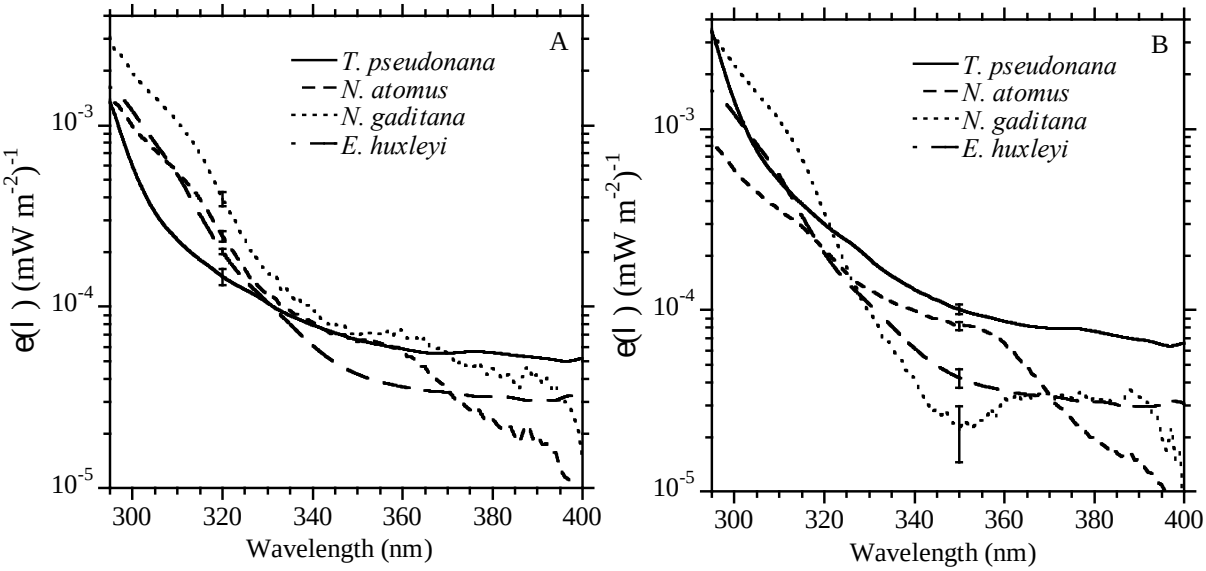

969
970